Available online at www.sciencedirect.com
SCIENCE DIRECT®
Computers & Fluids 34 (2005) 23–47
computers & fluids
www.elsevier.com/locate/compfluid

An investigation of turbulent open channel flow with heat transfer by large eddy simulation

Lei Wang, Yu-Hong Dong, Xi-Yun Lu *

Department of Modern Mechanics, University of Science and Technology of China, Hefei, Anhui 230026, PR China

Received 25 July 2003; received in revised form 19 February 2004; accepted 16 March 2004
Available online 20 July 2004

Abstract

Large eddy simulation of fully developed turbulent open channel flow with heat transfer is performed. The three-dimensional filtered Navier–Stokes and energy equations are numerically solved using a fractional-step method. Dynamic subgrid-scale (SGS) models for the turbulent SGS stress and heat flux are employed to close the governing equations. Two typical temperature boundary conditions, i.e., constant temperature and constant heat flux being maintained at the free surface, respectively, are used. The objective of this study is to explore the behavior of heat transfer in the turbulent open channel flow for different temperature boundary conditions and to examine the reliability of the LES technique for predicting turbulent heat transfer at the free surface, in particular, for high Prandtl number. Calculated parameters are chosen as the Prandtl number (Pr) from 1 up to 100, the Reynolds number (Re_τ) 180 based on the wall friction velocity and the channel depth. Some typical quantities, including the mean velocity, temperature and their fluctuations, heat transfer coefficients, turbulent heat fluxes, and flow structures based on the velocity, vorticity and temperature fluctuations, are analyzed.

1. Introduction

Understanding and prediction of the interaction of turbulence with a free surface and scalar transfer (e.g., heat and mass transfer) near a free surface are of great interest in both applications and fundamentals. It is needed to reveal more fundamental knowledge of scalar transport processes near interfacial surface and the interaction of turbulence with the surface. The structure of

* Corresponding author. Tel.: +86-551-3603223; fax: +86-551-3606459.
E-mail address: xlu@ustc.edu.cn (X.-Y. Lu).

0045-7930/$ - see front matter © 2004 Elsevier Ltd. All rights reserved.
doi:10.1016/j.compfluid.2004.03.004

turbulence is a key factor to the understanding of scalar transfer rates across interface because most of the resistance to the transfer is generally located just below the interface. This connection with heat and mass transfer problems has provided a strong motivation for clarifying the dynamical processes in the surface region and has led to many experimental and numerical investigations.

As well known, a natural and convenient way to investigate free surface turbulent flow is by use of fully developed turbulent open channel flow, where the turbulence that arrives at the free surface is produced principally at the bottom solid wall. Investigations on open channel turbulence have been performed experimentally and computationally and are briefly reviewed here. Some typical experiments [1–8] have revealed that the most surface renewal events are due to bursting processes near the solid boundary, and verified that large-scale, energy-containing eddies are primarily responsible for surface renewal. A relatively simple scenario emerges from these experiments; low-speed fluid is ejected toward the surface from the bottom wall burst, the fluid rises to the surface to form a surface renewal patch, and a downdraft develops after the interaction. Recently, experimental study [9] has used infrared technology to determine the relationship between the free surface temperature field and the subsurface velocity field and to identify the surface thermal signature of the thin thermal boundary layer.

Although those experiments have revealed much about the processes involved in turbulent surface renewal, considerable difficulty in making accurate velocity and scalar measurements very near the free surface appears. To some extent, an accurate numerical simulation can be employed to study this problem, allowing precise determination of the velocity field very close to the free surface. As well known, direct numerical simulation (DNS) is an efficient approach to analyze the behaviors of turbulence structure and scalar transport near the free surface. However, due to the expensive cost of the DNS, some typical previous work was only limited their investigations to low Reynolds number (usually $Re_\tau \leqslant 180$, defined by the wall friction velocity and the channel depth) and low or moderate Prandtl number ($Pr \leqslant 2$). The DNS calculations [10–13] have been performed to investigate turbulence structures near the free surface in an open channel flow with a zero-shear interface. Recently, some DNS work has been performed to investigate turbulence structure and scalar transport near the free surface in an open turbulent channel flow with a passive scalar. Nagaosa [14] studied the dynamics of well-organized tube-like coherent structures under a free surface and turbulent scalar transfer across the free surface for the turbulent open channel flow at $Re_\tau = 150$ and $Pr = 1$. Handler et al. [15] investigated fully developed turbulence in the open channel with passive heat transfer at $Re_\tau = 180$ and $Pr = 2$, and found the wake-like structure of the patches at the free surface as well as the importance of the interaction of turbulent structures in free surface with heat transport. In addition, Shen et al. [16,17] dealt with numerically and analytically the mixing of a passive scalar in turbulent shear flow with a free surface.

In the problem of heat transfer by fluid flow, the Prandtl number can be ranged from order of unity or less to hundreds. The fundamental mechanism and main statistical characteristics of the fluctuating heat transfer need to be understood. In the case of the heat transfer at low or moderate Prandtl number, a significant temperature gradient exists not only in the diffusive sublayer but also in the region outside the sublayer. High-Prandtl-number heat transfer is of special importance in the understanding of heat transfer near a free surface and in a turbulent boundary layer flow. The heat diffusive sublayer for the high-Prandtl-number heat transfer by the interface or boundary is very thin, and the heat transfer efficiency is primarily controlled by turbulent motions

very closing to the interface or boundary. The complexity of turbulence interactions near the interface results in unusual behaviors of heat transfer. Thus it is a challenging task to study the heat transfer at high Prandtl number.

It is obviously impossible to use DNS approach to solve problems in which both the Reynolds and Prandtl numbers are large, since the number of mesh points required to describe all the scales is of order $Pr^3Re^{9/4}$. However, it is now well established that large eddy simulation (LES) technique, which is much cheaper than the DNS since it solves only the large-scale components of turbulent flow and models the subgrid-scales (SGS) effects via SGS models, provides an effective tool to study some detailed features of turbulent flows. In the LES approach, the SGS model is a key problem. A dynamic SGS model was proposed by Germano et al. [18] which overcome some shortcomings of the classical Smagorinsky model [19]. The dynamic model gained a remarkable success in the past decade and it gave a new impetus to the development of new strategies for the LES [20–22]. Recently, an improved dynamic SGS model, including subgrid turbulent stress and heat flux models, for thermally stratified flow was proposed and applied to the thermally stratified turbulent channel flows for investigating the coupled shear and buoyancy effects on turbulent heat transfer [23,24]. On account of the improvements made by the SGS models, it becomes highly tempting to use the dynamic SGS model for studying turbulent flow with scalar transfer at high Prandtl or Schmidt numbers [22,25,26].

To obtain reliable LES results for turbulent flow and heat transfer in turbulent open channel flow, in particular, for high-Prandtl-number heat transfer, it is needed to ensure that replacing DNS by LES will not produce significant deviation in the large scales of turbulent and thermal fields. The LES approach, coupled with dynamic SGS turbulent stress and heat flux models, has been already employed to study fully developed turbulent two-walled channel flow with scalar transfer at high Prandtl and Schmidt number [22,25]. Comparison of the LES results with known turbulent statistics and well-established correlations for the scalar transfer rate have revealed a very good quantitative agreement at high Prandtl and Schmidt numbers. On the other hand, it is found that, since turbulence distortion is less severe near a free surface than near a solid wall, there is no doubt that the LES approach provides an accurate description of the large-scale dynamics in the surface-influenced region of an open channel flow [27,28]. Salvetti et al. [27] employed the LES technique to investigate decaying turbulence in an open channel without heat transfer and found that the LES approach is able to reproduce the features of the decay process observed in the direct simulation and to handle the anisotropic nature of the flow. Calmet and Magnaudet [28] performed the LES to deal with statistical characteristics of turbulence in the near surface region for a steady open channel flow without heat transfer. They revealed that the correct dissipation profile close to the surface being recovered through the LES calculation and confirmed that near-surface dissipation is essentially governed by viscous effects affecting the large-scale motions. Consequently, there seems to be no particular difficulty in reproducing correctly the large-scale turbulent and thermal fields in the free surface region by means of the LES approach.

Usually, a fully developed turbulent open channel flow is used as the basis in this study. The motivation is principally concerned with the relationship between turbulent structure and temperature field near the free surface. The turbulent open channel flows with two kinds of boundary condition for temperature at the free surface are investigated. The Prandtl number (Pr) ranges from 1 up to 100 and the Reynolds number (Re_τ) is 180 based on the wall friction velocity and the channel depth. The boundary conditions consist of both constant temperature and fixed heat flux

at the free surface. The three-dimensional resolved incompressible Navier–Stokes equations and the energy equation are solved simultaneously by the fractional-step method proposed by Kim and Moin [29], Verzicco and Orlandi [30]. Dynamic SGS models for SGS turbulent stresses and turbulent heat fluxes are used to closure the equations.

This paper is organized as follows. The mathematical formulations and the dynamic SGS models for modeling turbulent stresses and heat fluxes are described in Section 2. The numerical method and its validation are given in Section 3. In Section 4, statistical turbulence quantities and flow structures are discussed. Finally, concluding remarks are summarized in Section 5.

2. Mathematical formulations

To investigate heat transfer near a free surface for fully developed turbulent open channel flow in the absence of significant surface deformations or buoyancy effects, as schematically shown in Fig. 1, the three-dimensional filtered incompressible Navier–Stokes and energy equations are simultaneously solved. Two typical temperature boundary conditions at the free surface are used. One is that constant temperature is maintained at the free surface (hereafter, referred to as condition-1), and the other is that the interfacial heat flux is fixed at the free surface (condition-2). To non-dimensionalize the governing equations, the wall friction velocity u_τ is used as the velocity scale, the channel depth δ as the length scale. Further, $\Delta T = T_B - T_F$ for condition-1 and $q_0\delta/k$ for condition-2 are employed as the temperature scale, respectively, where T_B and T_F denote the temperature on the bottom wall and on the free surface, respectively, k represents the thermal conductivity, and q_0 is the magnitude of heat flux directed normal to the free surface. The non-dimensional governing equations are given as

$$\frac{\partial \bar{u}_i}{\partial x_i} = 0 \tag{1}$$

$$\frac{\partial \bar{u}_i}{\partial t} + \frac{\partial}{\partial x_j}(\bar{u}_i \bar{u}_j) = -\frac{\partial \bar{p}}{\partial x_i} + \frac{1}{Re_\tau}\frac{\partial^2 \bar{u}_i}{\partial x_j \partial x_j} - \frac{\partial \tau_{ij}}{\partial x_j} + \delta_{i1} \tag{2}$$

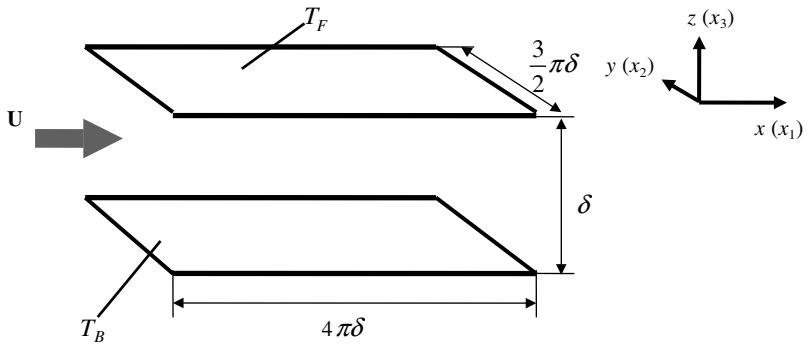

Fig. 1. Sketch of open channel flow with heat transfer.

$$\frac{\partial \overline{T}}{\partial t}+\frac{\partial(\overline{T}\bar{u}_j)}{\partial x_j}=\frac{1}{Re_\tau Pr}\frac{\partial^2\overline{T}}{\partial x_j\partial x_j}-\frac{\partial q_j}{\partial x_j} \tag{3}$$

where $\tau_{ij}=R_{ij}-\delta_{ij}R_{kk}/3$, $R_{ij}=\overline{u_iu_j}-\bar{u}_i\bar{u}_j$, $q_j=\overline{Tu}_j-\overline{T}\bar{u}_j$, overbar "–" represents the resolved variable. The Reynolds number Re_τ is defined as $Re_\tau=u_\tau\delta/\nu$, and the Prandtl number Pr as $Pr=\nu/\kappa$, where ν is the kinematic viscosity and κ is the thermal diffusivity of the fluid. $\bar{u}_i$ and $\overline{T}$ are the resolved velocity and temperature. $\bar{p}$ is the resolved modified pressure, which contains a term $R_{kk}/3$. The resolved velocity $\bar{u}_i$ $(i=1,2,3)$, for writing convenience, is represented as u, v and w in the streamwise (x), spanwise (y) and vertical (z) directions, respectively.

In Eqs. (2) and (3), τ_{ij} and q_j represent SGS turbulent stress and heat flux, respectively, which need to be modeled by SGS models. It is assumed that the heat transfer is a passive scalar that does not influence the flow dynamics. Thus the temperature depends on both Re_τ and Pr. The overall expressions of the SGS stresses and heat flux read, respectively

$$\tau_{ij}=-2C\overline{\Delta}^2|\overline{S}|\overline{S}_{ij},\qquad q_j=-\frac{C\overline{\Delta}^2}{Pr_{\mathrm{T}}}|\overline{S}|\frac{\partial\overline{T}}{\partial x_j} \tag{4}$$

where $\overline{S}_{ij}=(\partial\bar{u}_i/\partial x_j+\partial\bar{u}_j/\partial x_i)/2$, $|\overline{S}|=[2\overline{S}_{ij}\overline{S}_{ij}]^{1/2}$. $\overline{\Delta}$ is the filter width, and Pr_{T} represents the turbulent Prandtl number.

Here, the model coefficients of C and Pr_{T} in Eq. (4) are obtained by use of the approach proposed by Germano et al. [18]. After introducing a test filtering with a filter width $\hat{\overline{\Delta}}$ to Eqs. (1)–(3), the coefficients C and Pr_{T} can be dynamically determined as

$$C=-\frac{1}{\overline{\Delta}^2}\frac{\langle L_{ij}M_{ij}\rangle_S}{\langle M_{ij}M_{ij}\rangle_S},\qquad Pr_{\mathrm{T}}=-C\overline{\Delta}^2\frac{\langle F_iF_i\rangle_S}{\langle E_iF_i\rangle_S} \tag{5}$$

where $M_{ij}=2\alpha^2|\hat{\overline{S}}|[\hat{\overline{S}}_{ij}-\frac{1}{3}\hat{\overline{S}}_{kk}\delta_{ij}]-\hat{m}_{ij}$, $L_{ij}=\hat{\bar{u}_i\bar{u}_j}-\hat{\bar{u}}_i\hat{\bar{u}}_j-\frac{1}{3}(\hat{\bar{u}_k\bar{u}_k}-\hat{\bar{u}}_k\hat{\bar{u}}_k)\delta_{ij}$, $m_{ij}=2|\overline{S}|\left[\overline{S}_{ij}-\frac{1}{3}\overline{S}_{kk}\delta_{ij}\right]$, $E_i=\hat{\bar{u}}_i\hat{\overline{T}}-\hat{\bar{u}_i\overline{T}}$, $F_i=\alpha^2|\hat{\overline{S}}|\hat{B}_i-|\overline{S}|\hat{B}_i$, and $B_j=\partial\overline{T}/\partial x_j$.

Here, $\alpha=\hat{\overline{\Delta}}/\overline{\Delta}$ is chosen as 2 in the present calculation, $\langle\rangle_S$ denotes some kind of spatial averaging to remove the calculation oscillation [18]. In the present calculation, the average is taken in the plane parallel to the wall plate [25–28].

At the bottom wall $z=0$, no-slip and no-penetration velocity conditions are imposed. The boundary conditions applied at $z=1$ are those for a shear-free interface without deformation,

$$\bar{w}=0,\qquad \frac{\partial\bar{u}}{\partial z}=\frac{\partial\bar{v}}{\partial z}=0 \tag{6}$$

The flow and temperature fields are assumed to be statistically homogeneous in the streamwise and spanwise directions. Thus, periodic boundary conditions are used in both the directions. For condition-1, two different constant temperatures, with the bottom temperature being greater than the free surface, are imposed on the free surface and the bottom wall,

$$\overline{T}=T_{\mathrm{F}}=0,\quad \text{at } z=1;\qquad \overline{T}=T_{\mathrm{B}}=1,\quad \text{at } z=0 \tag{7}$$

For condition-2, constant heat flux, directed out of the top boundary, is set at the free surface, and constant temperature is maintained on the bottom wall,

$$\partial\overline{T}/\partial z=-1,\quad \text{at } z=1;\qquad \overline{T}=T_{\mathrm{B}}=0,\quad \text{at } z=0 \tag{8}$$

Heat transfer computation is started after the flow field has statistically reached fully developed turbulent state. Initial temperature field is set to be a linear distribution along the z-direction (i.e., $\overline{T} = 1 - z$ and $\overline{T} = -z$ for the condition-1 and condition-2, respectively) and homogeneous in the horizontal planes.

3. Numerical methods

To perform LES calculation, a fractional-step method developed by Kim and Moin [29] and Verzicco and Orlandi [30] is employed to solve Eqs. (1)–(3). Spatial derivatives are discretized by a second order central difference. Time advancement is carried out by the semi-implicit scheme using the Crank–Nicolson scheme for the viscous terms and the three-stage Runge–Kutta scheme for the convective terms. The low-storage Runge–Kutta methods have the additional advantage that the minimum amount of computer run-time memory is realized. The discretized formulation was described in detail by Verzicco and Orlandi [30] and Verzicco and Camussi [31].

In this study, the size of computational domain is $4\pi\delta \times 3\pi\delta/2 \times \delta$ with the corresponding grid number $97\times97\times97$ in the streamwise, spanwise and vertical directions, respectively. The domain size is chosen such that two-point correlations in both the streamwise and spanwise directions are negligibly small. The grid independence of the present calculation has been ensured for every simulation. The grid is uniform along both the streamwise and spanwise directions. In the vertical direction, to increase the grid resolution near the top free surface and bottom wall, respectively, the grid distribution is stretched so that it is sufficient to resolve the viscous sublayer and diffusive sublayer near the boundary [32,33]. The grid spacing is determined by the requirement that at least three points are within the diffusive sublayer near each boundary [25,26].

To verify the performance of the present LES calculation at high Prandtl number, a typical case is considered for fully developed turbulent two-walled channel flow with passive heat transfer at $Pr = 100$ and $Re = 10^4$ based on the centerline mean velocity and the half-width of the channel. Fig. 2 shows the profile of the mean temperature normalized by the friction temperature. Experimental and computational data [34] at $Pr = 95$ with the same Reynolds number are also given in Fig. 2. Although the Prandtl number in the present calculation is somewhat different from that in [34], both results are reasonably in good agreement with each other.

Moreover, extensive validations and verifications relevant to the present code have been performed in our previous work, including thermally stratified turbulent channel flow [23,24], turbulent channel flows with passive scalar transfer [25,26], oscillating turbulent boundary layer flow [35], oscillating turbulent channel flow with heat transfer [36], and thermally stratified turbulent channel flow with temperature oscillation [37]. It can be confirmed that our calculation is reliable for the prediction of statistical quantities of the turbulent flow and heat transfer. To further validate and verify the present calculation for turbulent open channel flow with heat transfer near a free surface, some quantitative comparison will be given in the following section.

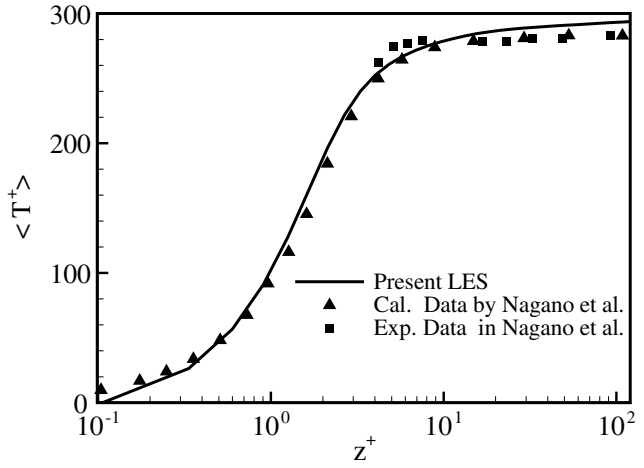

Fig. 2. Profile of the mean temperature for turbulent two-walled channel flow with passive heat transfer at $Pr = 100$ and comparison with experimental and computational data [34].

4. Results and discussion

4.1. Velocity statistics

As turbulent open channel flow with passive heat transfer is considered, the velocity and temperature fields are uncoupled. Fig. 3 shows the mean streamwise velocity versus z_B^+ at $Re_\tau = 180$, where z_B^+ is the vertical distance from the bottom wall normalized by the friction velocity and is defined as $z_B^+ = zu_\tau/v$. Based on previous investigations [12–15], the velocity

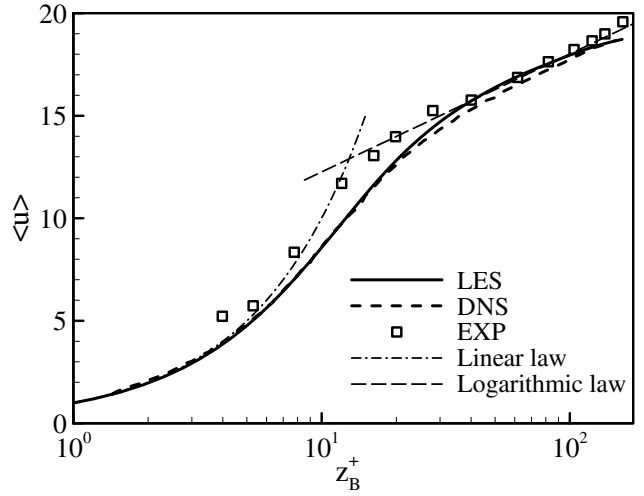

Fig. 3. Profile of the mean streamwise velocity for turbulent open channel flow at $Re_\tau = 180$ and comparison with experimental data [10] and computational result [15].

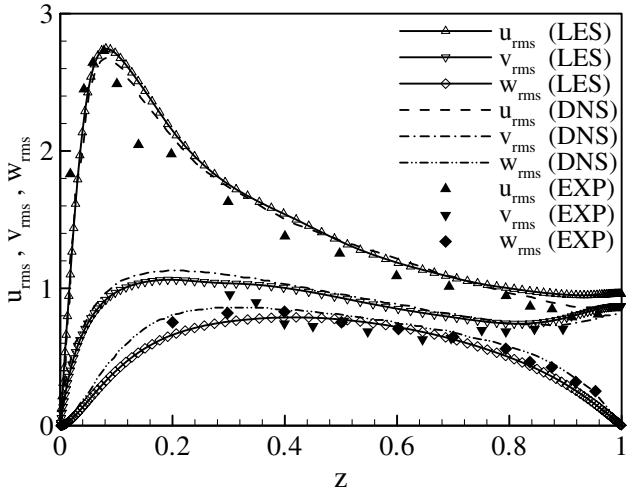

Fig. 4. Profiles of the root-mean-square velocity at $Re_\tau = 180$ and comparison with experimental data [10] and DNS result [15].

statistics near the no-slip boundary are not affected by the existence of a free surface. From Fig. 3, there exists a buffer layer followed by a standard logarithmic region in the mean velocity profile, which is closely similar to that of fully developed turbulent two-walled channel flow. However, there is a slight deviation from the classic logarithmic region in the wall law for $z_B^+ > 100$ which must be assumed to be due to the presence of the free surface. To validate and verify quantitatively the present calculation, some typical experimental data [10] and DNS result [15] are also plotted in Fig. 3; our calculated results are in good agreement with them.

The profiles of turbulence intensity, i.e., the root-mean-square values of the streamwise, spanwise and vertical velocity fluctuations (u_{rms}, v_{rms} and w_{rms}), are shown in Fig. 4. The turbulence intensities exhibit characteristics near the bottom wall being in agreement with standard two-walled channel flow [25,32] and show a strong anisotropy near the shear-free boundary. Based on the analysis of the turbulence kinetic energy, the mechanism of the strong anisotropy near the free surface is closely related to the effect of the pressure–strain on the energy transfer [38]. Meanwhile, it is noted that our calculated result agrees well with the experimental data [10] and DNS result [15].

4.2. Temperature statistics

To further validate the present LES of fully developed turbulent open channel flow with heat transfer for both the temperature conditions in Eqs. (7) and (8), Fig. 5 shows the mean temperature (T_F^+) versus the vertical distance (z_B^+) at $Pr = 2$, where T_F^+ represents the temperature normalized by the friction temperature at the free surface. It is found that our calculated results for both the temperature conditions at the free surface agree well with the DNS data [15]. Some typical validation for high Pr numbers has been given in Fig. 2 and in our previous work [25,26]; it is confirmed that the present LES calculation can reasonably predict turbulent heat transfer at high Pr number.

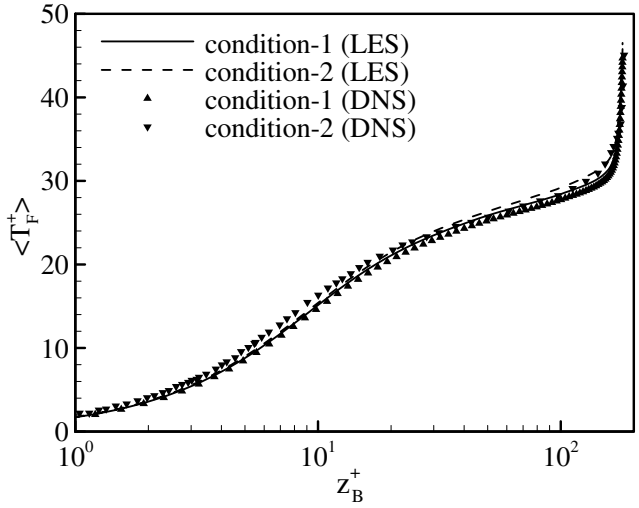

Fig. 5. Profile of the mean temperature at $Pr = 2$ and comparison with DNS data [15].

To exhibit the global behavior of the mean temperature over the vertical channel, Fig. 6 shows the profiles of the mean temperature. The distributions of the mean temperature for condition-1 (Fig. 6a) and condition-2 (Fig. 6b) are obviously different for the same Pr number. The diffusive sublayer becomes thinner and thinner with the increase of Pr number. Shaw and Hanratty [43] investigated experimentally and theoretically on fully developed turbulent wall flow with heat transfer, and proposed that the diffusive sublayer thickness at different Pr numbers were related approximately by the $Pr^{-1/3}$ law predicted theoretically [39] and by the $Pr^{-0.3}$ law proposed experimentally [43]. It is easy to find that the values of the diffusive sublayer thickness near the bottom wall for different Pr numbers are very close to those laws $Pr^{-1/3}$ or $Pr^{-0.3}$. The character is consistent with the two-walled turbulent channel flow with heat transfer [25]. Meanwhile, by checking Fig. 6, the diffusive sublayer near the free surface is thinner than that near the bottom wall for the same Pr number. Here, it is interesting to note that the values of the diffusive sublayer thickness near the free surface are related by the law $Pr^{-1/2}$ approximately in consistent with the prediction of standard surface renewal model [6].

As shown in Fig. 6, the mean temperature at the free surface (denoted by T_{F0}) varies with Pr number for condition-2 and its distribution is shown in Fig. 7. It is reasonably predicted that the mean surface temperature increases with the increase of Pr. As a typical case, compared to the surface temperature at $Pr = 2$ obtained by the DNS [15], the present calculated surface temperature at $Pr = 2$ is -0.1335 approximately, which agrees well with the DNS data -0.133.

The profiles of the mean temperature, normalized by the friction temperature, near the bottom wall are shown in Fig. 8 versus $z_B^+ = zu_\tau/\nu$ in logarithmic scale. Here, the mean temperature is given as

$$\langle T_B^+ \rangle = [T_B - \langle \overline{T}(z) \rangle]/T_B^\tau \tag{9a}$$

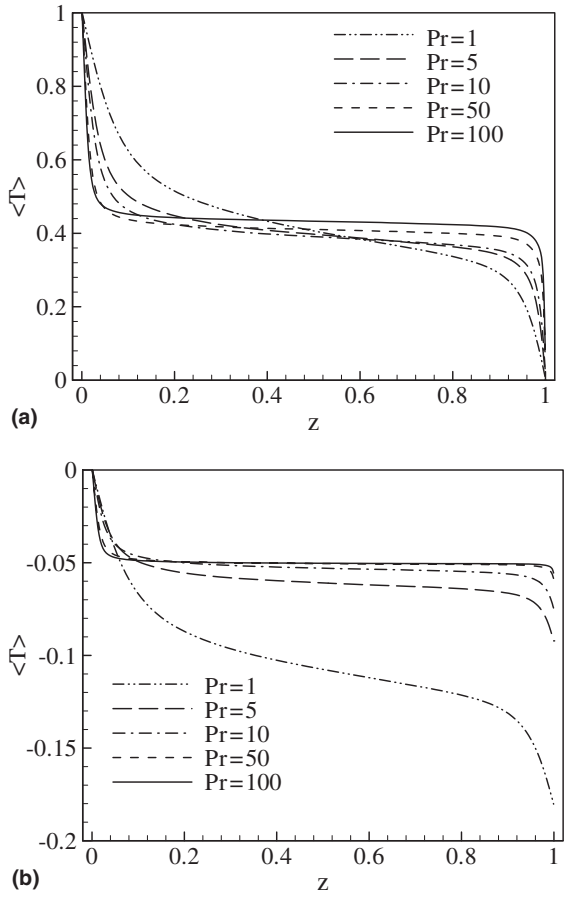

Fig. 6. Distributions of the mean temperature for different Prandtl numbers in global coordinate: (a) condition-1; (b) condition-2.

where T_{B}^{τ} is the friction temperature at the bottom wall and is defined as

$$T_{\mathrm{B}}^{\tau} = \frac{\kappa}{u_{\tau}} \left| \frac{\partial \langle \overline{T} \rangle}{\partial z} \right|_{z=0} \tag{9b}$$

From Fig. 8a and b, it is noted that the mean temperature profiles near the bottom wall for condition-1 (Fig. 8a) and condition-2 (Fig. 8b) are similar with each other for the same *Pr* number. Thus, the temperature statistics near the no-slip boundary are nearly not affected by the existence of a free surface with different temperature conditions. Such the behavior is similar to the mean velocity profile in Fig. 3 and the previous findings [12–15].

Similar to the mean velocity distribution, there exists a buffer layer followed by a logarithmic region in the mean temperature profile near the bottom wall in Fig. 8, where, $\langle T_{\mathrm{B}}^{+} \rangle$ behaves as

$$\langle T_{\mathrm{B}}^{+} \rangle = \beta_1(Pr) z_{\mathrm{B}}^{+} \tag{10a}$$

$$\langle T_{\mathrm{B}}^{+} \rangle = \alpha \ln z_{\mathrm{B}}^{+} + \beta_2(Pr) \tag{10b}$$

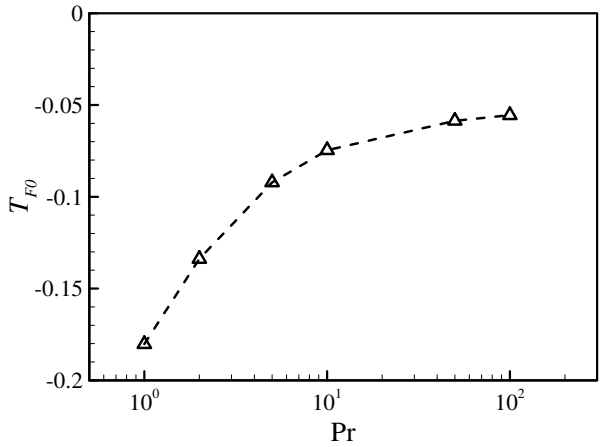

Fig. 7. Mean surface temperature at the free surface for condition-2 versus the Prandtl number.

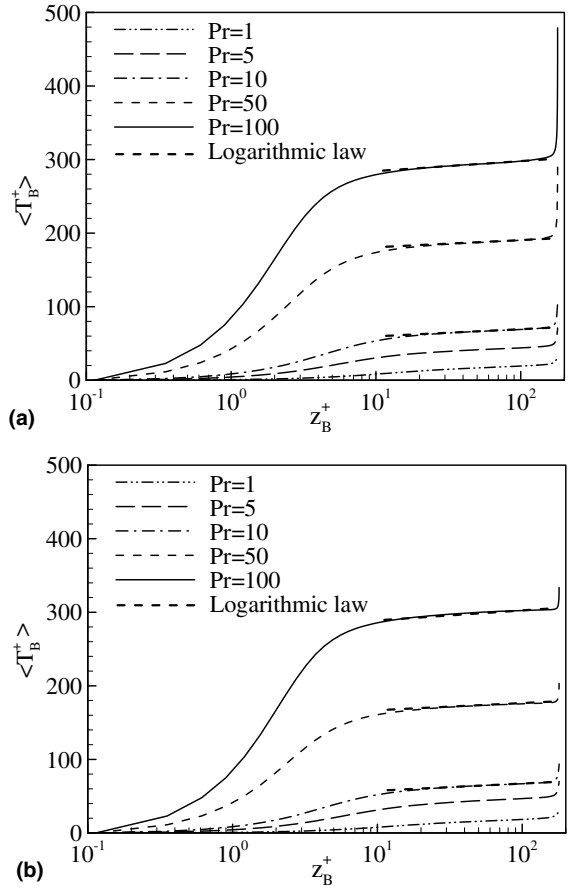

Fig. 8. Profiles of the mean temperature near the bottom wall: (a) condition-1; (b) condition-2.

where $1/\alpha$ represents the von Karman constant for the mean temperature profile, β_1 and β_2 do not vary with z_B^+ but change with the Prandtl number. Kader and Yaglom [39] found $\alpha = 2.12$ approximately while Kader [40] gave an empirical expression for the function β_2 that describes the experimental results in the logarithmic region of the fully turbulent boundary layer. The curve of (10b) is plotted in Fig. 8. The slope of α is approximately constant for several *Pr* numbers, almost independent of the Prandtl number. This means that the z_B^+-logarithmic plots of the mean temperature profile near the bottom wall may be nearly parallel for different *Pr* numbers, which was also confirmed by Kawamura et al. [41,42] based on DNS calculation for two-walled turbulent channel flow with passive heat transfer.

Correspondingly, the profiles of the mean temperature near the free surface are shown in Fig. 9 versus $z_F^+ = (1-z)u_\tau/\nu$ in logarithmic scale. Here, the mean temperature, normalized by the friction temperature, is represented as

$$\langle T_F^+ \rangle = [\langle \overline{T}(z) \rangle - T_F^*]/T_F^\tau \tag{11a}$$

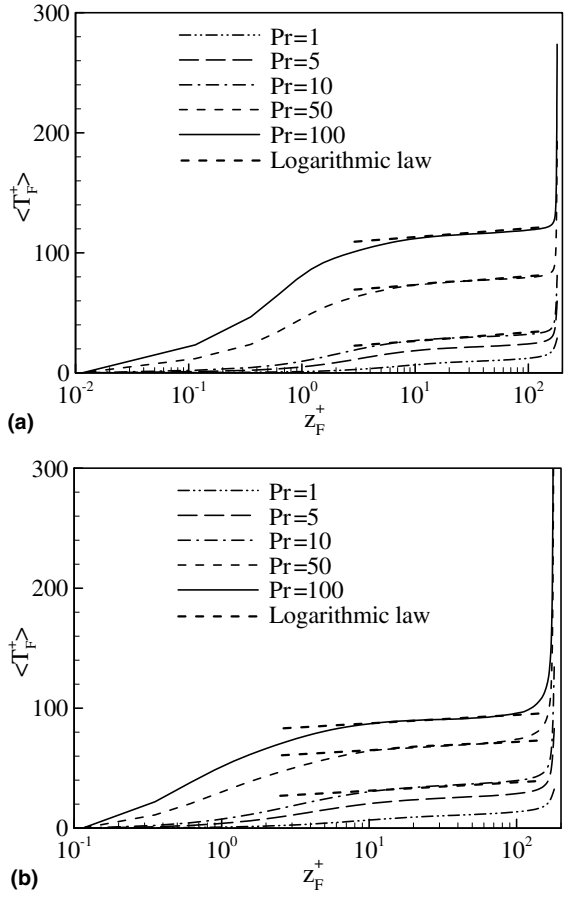

Fig. 9. Profiles of the mean temperature near the free surface: (a) condition-1; (b) condition-2.

where T_F^* is the temperature at the free surface and is represented as $T_F^* = T_F = 0$ from Eq. (7) for condition-1 and as $T_F^* = T_{F0}$ from Fig. 7 for condition-2, and T_F^τ denotes the friction temperature at the free surface and is defined as

$$T_F^\tau = \frac{\kappa}{u_\tau}\left|\frac{\partial\langle\overline{T}\rangle}{\partial z}\right|_{z=1} \tag{11b}$$

Based on the normalization in (11), it is noted that the mean temperature profiles near the free surface for condition-1 (Fig. 9a) and condition-2 (Fig. 9b) are very similar with each other for the same *Pr* number. Meanwhile, as shown in Fig. 9, the z_F^+-logarithmic plots of the mean temperature profile in the logarithmic region near the free surface is nearly parallel for different *Pr* numbers and also behaves as $\langle T_F^+\rangle = \alpha \ln z_F^+ + \beta_3(Pr)$ which is similar to (10b), where β_3 does not vary with z_F^+ but change with *Pr*.

Further, the behavior of the mean temperature fluctuation is analyzed. Fig. 10 shows the profiles of the mean temperature fluctuation normalized by the friction temperature at the bottom

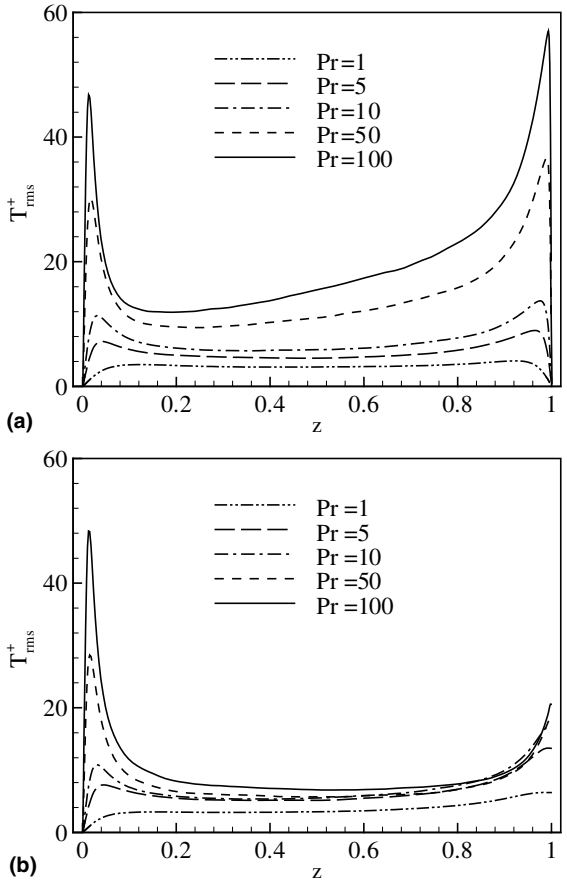

Fig. 10. Profiles of the mean temperature fluctuation: (a) condition-1; (b) condition-2.

wall (i.e., T_B^{τ}). As shown in Fig. 10a for condition-1, the peak value of the temperature fluctuation near the free surface is higher than that near the bottom wall. As *Pr* increases, the peak value near the free surface (or near the wall) increases and its position moves towards the free surface (or towards the wall). In the near wall region, the results appear to be in reasonable agreement with those of turbulent two-walled channel flow [25,26]. As the distance from the free surface goes to 0, the temperature fluctuations near the free surface approach to 0 linearly with a slope varying with *Pr* as shown in Fig. 10a. However, the temperature fluctuation at the free surface is not 0 in Fig. 10b for condition-2, and its value increases with the increase of *Pr*.

4.3. Thermal statistics

To deal with the Prandtl number dependence of the mean turbulent heat transfer coefficients near the free surface and near the bottom wall, the mean turbulent heat transfer coefficients versus *Pr* are exhibited in Fig. 11. Here, the mean turbulent heat transfer coefficients, K_F^+, near the free surface, and K_B^+, near the bottom wall, respectively, are defined as

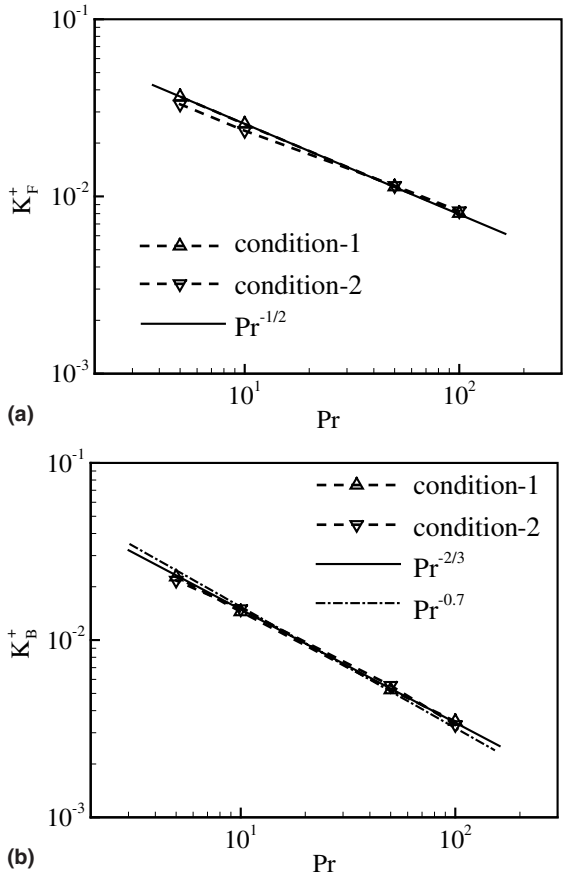

Fig. 11. Mean turbulent heat transfer coefficients: (a) near the free surface; (b) near the bottom wall.

$$K_{\mathrm{F}}^{+}=\frac{\kappa}{u_{\tau}\Delta T_{\mathrm{CF}}}\left|\frac{\partial\langle\overline{T}\rangle}{\partial z}\right|_{z=1},\qquad K_{\mathrm{B}}^{+}=\frac{\kappa}{u_{\tau}\Delta T_{\mathrm{CB}}}\left|\frac{\partial\langle\overline{T}\rangle}{\partial z}\right|_{z=0} \tag{12}$$

where ΔT_{CF} and ΔT_{CB} represent the temperature difference between the core of the channel and the free surface and between the bottom wall and the core of the channel, respectively.

Actually, there have been very few reliable measurements of heat transport in open channel flows in the absence of surface shear [15]. Based on the finding of experiment [3], the mean turbulent heat transfer coefficient near the free surface should vary in proportion to $Pr^{-0.5}$, i.e., $K_{\mathrm{F}}^{+}\sim Pr^{-0.5}$, in accordance with standard surface renewal model [7]. As shown in Fig. 11a, it is verified numerically that the turbulent heat transfer coefficient near the free surface agrees well with the $Pr^{-0.5}$ law. On the other hand, Kader and Yaglom [39] suggest the Pr dependence of K_{B}^{+} as $K_{\mathrm{B}}^{+}\sim Pr^{-2/3}$ as $Pr\to\infty$ for fully developed turbulent wall flow with heat transfer. Shaw and Hanratty [43] found $K_{\mathrm{B}}^{+}\sim Pr^{-0.7}$ from their experiment. As depicted in Fig. 11b, the turbulent heat transfer coefficient K_{B}^{+} near the bottom wall obeys approximately the $Pr^{-0.7}$ law predicted experimentally [43] and the $Pr^{-2/3}$ law proposed theoretically [39].

To explore the character of the mean turbulent heat transfer, Figs. 12 and 13 show the profiles of the mean streamwise and vertical turbulent heat fluxes in the vicinity of the free surface for condition-1 and condition-2, respectively. Note that the temperature fluctuation in the turbulent heat fluxes is normalized by the friction temperature at the free surface (T_{F}^{τ}). Near the free surface, the temperature diffusive sublayer thickness becomes thinner with the increase of Pr in Fig. 6, and the corresponding temperature fluctuation is higher. Thus, as Pr increases, the heat fluxes by turbulent transport $\langle u'T'\rangle$ and $\langle w'T'\rangle$ become increasingly significant in the region near the free surface in Figs. 12 and 13.

Furthermore, considering the shear-free condition (6) and temperature condition (7), i.e., condition-1, the turbulent heat fluxes $\langle u'T'\rangle$ and $\langle w'T'\rangle$ can be expanded into power series of z_{F}^{+} in the vicinity of the free surface,

$$\langle u'T'\rangle=a_1z_{\mathrm{F}}^{+}+a_2z_{\mathrm{F}}^{+^2}+\cdots \tag{13a}$$

$$\langle w'T'\rangle=b_1z_{\mathrm{F}}^{+^2}+b_2z_{\mathrm{F}}^{+^3}+\cdots \tag{13b}$$

Then, both curves of the linear and square laws with the vertical distance from the free surface, z_{F}^{+}, are plotted in Fig. 12 with logarithmic scales to illustrate the first terms in (13). The turbulent heat fluxes in the streamwise and vertical directions agree well with the leading term behavior in (13) near the free surface, respectively.

Correspondingly, based on the conditions (6) and (8), i.e., condition-2, the turbulent heat fluxes $\langle u'T'\rangle$ and $\langle w'T'\rangle$ can be expanded into power series of z_{F}^{+} near the free surface,

$$\langle u'T'\rangle=c_1+c_2z_{\mathrm{F}}^{+}+\cdots \tag{14a}$$

$$\langle w'T'\rangle=d_1z_{\mathrm{F}}^{+}+d_2z_{\mathrm{F}}^{+^2}+\cdots \tag{14b}$$

In Fig. 13a, curve of the linear law with the vertical distance from the free surface is plotted to exhibit the first terms in (14b). From Eq. (14a), it is seen that the streamwise heat flux near the free surface, as shown in Fig. 13b, does not vary with z_{F}^{+} but change with Pr.

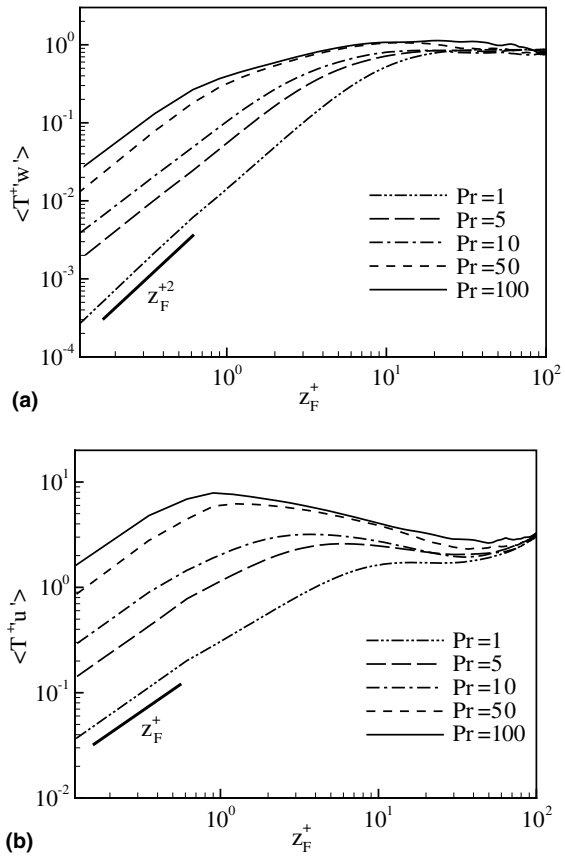

Fig. 12. Mean turbulent heat fluxes near the free surface for condition-1: (a) vertical component; (b) streamwise component.

The profiles of the mean streamwise and vertical turbulent heat fluxes near the bottom wall are shown in Fig. 14. Here, the temperature fluctuation in the turbulent heat fluxes is normalized by the friction temperature at the wall (T_B^τ). The heat fluxes increase significantly near the wall as the increase of Pr. Similarly, the turbulent heat fluxes $\langle u'T'\rangle$ and $\langle w'T'\rangle$ can be also expressed as power series of z_B^+ in the vicinity of wall,

$$\langle u'T'\rangle = e_1 z_B^{+^2} + e_2 z_B^{+^3} + \cdots \tag{15a}$$

$$\langle w'T'\rangle = g_1 z_B^{+^3} + g_2 z_B^{+^4} + \cdots \tag{15b}$$

Fig. 14 also depicts the curves of the square and cubic laws with z_B^+ to exhibit the first terms in (15). Although the effect of the free surface appears, it is evident that the turbulent heat fluxes are still in good agreement with the leading term character in (15) in the vicinity of the wall.

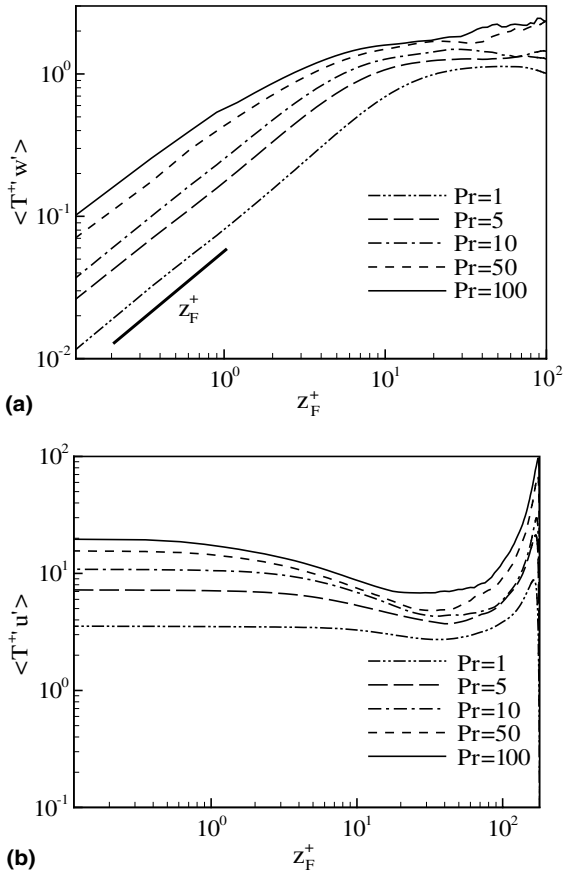

Fig. 13. Mean turbulent heat fluxes near the free surface for condition-2: (a) vertical component; (b) streamwise component.

4.4. Structures based on the velocity and temperature fluctuations

To explore the processes involved in the transport of heat at the free surface, it is needed to investigate the velocity and temperature fluctuations. It is evident that the heat flux at the free surface will vary spatially and temporally, its structure being determined by the velocity and temperature fields. It is known that eruption process of fluid from the bottom wall region usually retains their coherence in the sequence of convecting toward the free surface [6–8]. To understand these events near the free surface and indicate the activity of the turbulence near the free surface, both velocity and vorticity fields are discussed. Fig. 15a shows a top view of the contours of the vertical velocity fluctuation close to the free surface at $z_F^+ = 0.1$ approximately. The upward process eventually reaches the free surface as so-called "splatting events" and corresponds to the positive vertical velocity (solid lines) in Fig. 15a. Meanwhile, continuity requires antisplatting or descending motions from the surface. Thus, antisplatting events are usually encountered on the free surface and correspond to the negative vertical velocity (dashed lines) in Fig. 15a.

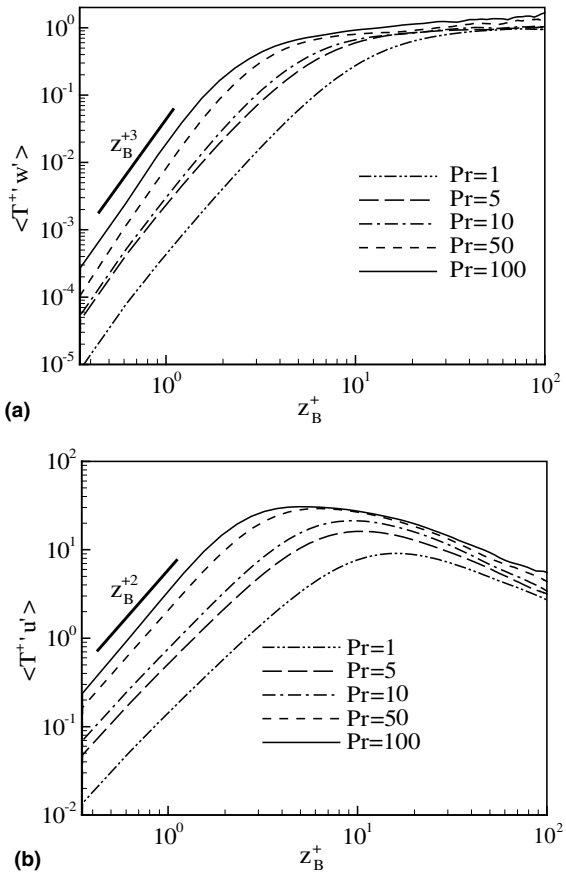

Fig. 14. Mean turbulent heat fluxes near the bottom wall: (a) vertical component; (b) streamwise component.

To clearly depict the regions of the splatting and antisplatting events, a local region marked by a solid-line square in Fig. 15a is chosen. Fig. 15b and c shows the enlarged patterns for the contours of the vertical velocity fluctuation and the vectors based on the streamwise and spanwise velocity fluctuations in the local region. Fig. 15b corresponds to the region of the splatting events, where the diverged velocity vectors with a positively large vertical velocity fluctuation are observed on the free surface. This structure contributes to the intercomponent energy transfer from vertical to the free surface parallel direction by pressure–strain effects. Fig. 15c exhibits the region of the antisplatting events, where the converged velocity vectors with a negatively large vertical velocity fluctuation are displayed. The splatting and antisplatting events play as an important role for the turbulent energy transfer between the vertical direction and the free surface parallel direction.

To demonstrate the structure in the regions of the splatting and antisplatting events, Fig. 16a shows the streamwise vorticity contours and the velocity vectors in the spanwise-vertical (i.e., y–z) plane along the line AB indicated in Fig. 15a. It clearly demonstrates that the organized structure near the free surface represents as "dipole vorticity", where two vortices are aligned

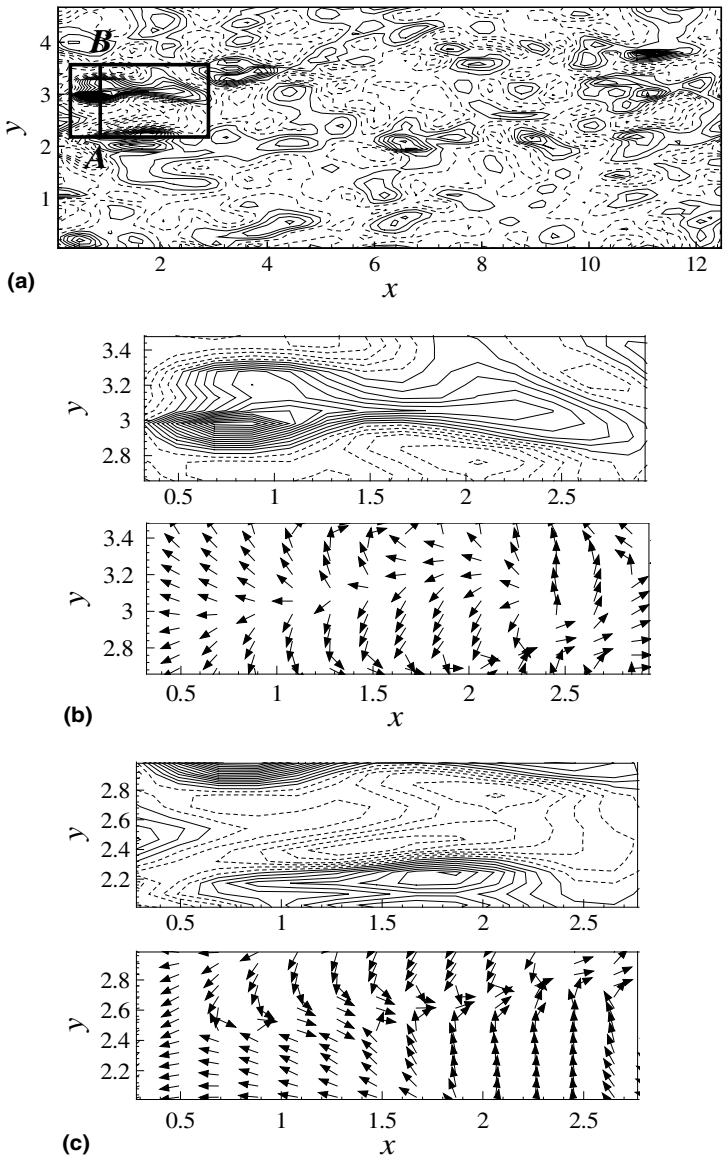

Fig. 15. Patterns of the instantaneous velocity fluctuations: (a) w' contours at $z_F^+ = 0.1$; (b) w' contours (upper) and $u' - v'$ vectors (lower) in the splatting region; (c) w' contours (upper) and $u' - v'$ vectors (lower) in the antisplatting region. Here, u', v' and w' represent the velocity fluctuations in the streamwise, spanwise and vertical directions.

along the streamwise direction. The vertical velocity fluctuation is quite large between both the vortices, and the positively large vertical velocity region corresponds to the splatting zone in Fig. 15b.

Based on the structure visualized in Fig. 16a, a sketch of the dynamics of the splattings is simply depicted in Fig. 16b. It can be proposed that the splattings are the result of the complicated

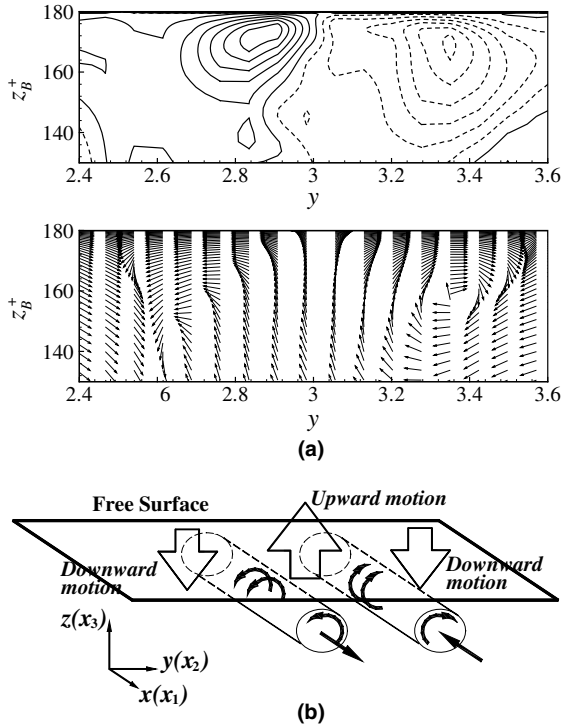

Fig. 16. Organized structure near the free surface: (a) streamwise vorticity contours (upper) and $v' - w'$ vectors (lower); (b) sketch of the organized structure.

interaction between the streamwise vortices. As the vortices are mainly aligned the streamwise direction, therefore the structures hardly transfer turbulence energy to the streamwise direction, which was confirmed based on the turbulent budget analysis [38]. The organized structure near the free surface usually corresponds to the surface renewal motion [3], patchy structure [7], and hairpin-like eddies near the free surface [15]. The splatting can replace the free surface fluid with fluid from the bulk due to the rotating motion of the vortices, corresponding to the upward flow as shown in Fig. 16. In addition, when heat transfer is considered, the heat can be transported from the wall toward the free surface due to the upward flow. Thus the upward fluid elements carry them with the higher temperatures associated with the subsurface flow, and must therefore be significantly warmer than the average surface temperature to form the so-called "hot spots" [15]. Therefore, it can be suggested that the splatting events should correspond to the hot spots near the free surface.

The instantaneous temperature fluctuation near the free surface in a cross plane y–z_F^+ at $Pr = 1$, 10 and 100 are shown in Fig. 17 for condition-1. The high- and low-temperature streaks are visualized in the region near the free surface. The structure scale of the temperature fluctuation decreases with the increase of Pr, and these structures spread over the region near the free surface. Correspondingly, Fig. 18 shows the instantaneous temperature fluctuation near the free surface in

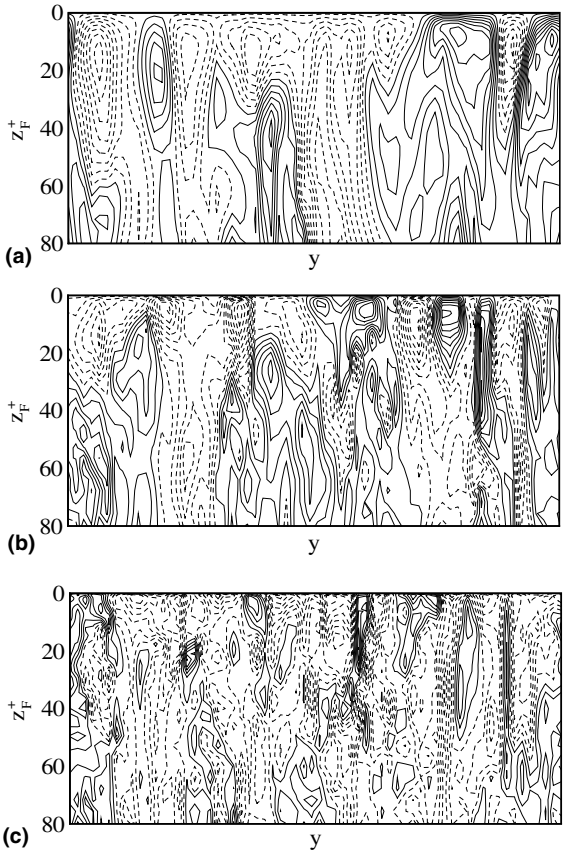

Fig. 17. Contours of the instantaneous temperature fluctuation near the free surface in a cross plane for condition-1: (a) $Pr = 1$; (b) $Pr = 10$; (c) $Pr = 100$.

a cross plane y–z_F^+ at $Pr = 1$, 10 and 100 for condition-2. The corresponding high- and low-temperature streaks are observed in the region near the free surface. The structure scale of the temperature fluctuation over the region also decreases with the increase of Pr. The temperature fluctuation contours end at the free surface in Fig. 18 because of the effect of the boundary condition at the free surface.

By viewing the structures in Figs. 17 and 18, it can be understood that these organized streaks of the temperature fluctuation are closely related with the structure of turbulence near the free surface, which are also connected with bursting processes near the wall. The temperature field is affected by both the free surface and bursting processes from the wall, and the organized streaks of the temperature fluctuation spread over the viscous sublayer and surface-influenced layer [22,25]. It is reasonably believable that the surface-influenced layer may play an important role in thermal transfer near the free surface and the anisotropy of the turbulence and the intercomponent energy transfer mainly happen within the surface-influenced layer.

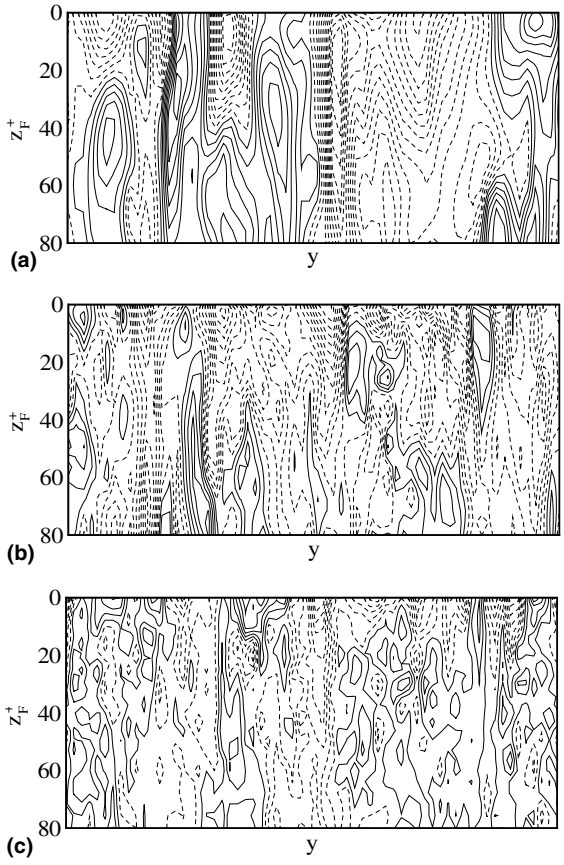

Fig. 18. Contours of the instantaneous temperature fluctuation near the free surface in a cross plane for condition-2: (a) $Pr = 1$; (b) $Pr = 10$; (c) $Pr = 100$.

5. Concluding remarks

Large eddy simulation of fully developed turbulent open channel flow with heat transfer is performed with two typical temperature boundary conditions at the free surface. The decisive validation of the present approach has been achieved by comparing our calculated results with some available computational, theoretical and experimental results, in particular for high-Prandtl-number flow. The behavior of heat transfer in the turbulent open channel flow for different temperature boundary conditions is analyzed.

The profiles of the mean temperature and its fluctuation near the free surface and the bottom wall have been examined for different Pr numbers. There exists a buffer layer followed by a logarithmic region in the mean temperature profiles, and the plots of the mean temperature profiles in the logarithmic region may be nearly parallel for different Pr numbers. The temperature fluctuation in the near regions of the free surface and the wall is strengthened with the increase of Pr. The mean diffusive sublayer thickness and turbulent heat transfer coefficient K_B^+ in the vicinity of the bottom wall behave like $Pr^{-1/3}$ and $Pr^{-2/3}$ as predicted theoretically [39], or approximately

like $Pr^{-0.3}$ and $Pr^{-0.7}$ as found experimentally [43]. Correspondingly, the mean turbulent heat transfer coefficient K_F^+ near the free surface varies as $Pr^{-0.5}$, in accordance with experimental finding [3] and standard surface renewal model [7]. It is verified that the mean streamwise and vertical turbulent heat fluxes vary in the manners of z_F^+ and z_F^{+2} for condition-1 as well as of z_F^{+0} and z_F^+ for condition-2, respectively, near the free surface, and in the manners of z_B^{+2} and z_B^{+3} near the bottom wall. Based on the structures of the instantaneous velocity and temperature fluctuations, it is demonstrated that the splatting and antisplatting events play as an important role for the turbulent energy transfer between the vertical direction and the free surface parallel direction. The presence of dipole streamwise vorticies is numerically verified. These vorticies contribute to the surface renewal at the free surface, control heat transfer, and induce strong anisotropic turbulent flow near the free surface.

Acknowledgements

This work was supported by the National Science Fund for Distinguished Scholars (no. 10125210), the China NKBRSF Project (no. 2001CB409600), the Hundred-Talent Programme of the Chinese Academy of Sciences, and Specialized Research Fund for the Doctoral Program of Higher Education (no. 20020358013).

References

[1] Nakagawa H, Nezu I. Structure of space–time correlations of bursting phenomena in open-channel flow. J Fluid Mech 1981;104:1–43.
[2] Komori S, Ueda H, Fumimaru O, Mizushina T. Turbulence structure and transport mechanism at a free surface in an open channel flow. Int J Heat Mass Transfer 1982;25:513–23.
[3] Komori S, Murakami Y, Ueda H. The relationship between surface-renewal and bursting motions in an open-channel. J Fluid Mech 1989;203:103–23.
[4] Komori S, Nagaosa R, Muramami Y. Turbulence structure and mass transfer across a sheared air–water interface in wind driven turbulence. J Fluid Mech 1993;249:161–83.
[5] Kumar S, Gupta R, Banerjee S. An experimental investigation of the characteristics of free-surface turbulence in channel flow. Phys Fluids 1998;10:437–56.
[6] Rashidi M, Banerjee S. Turbulence structure in free surface flows. Phys Fluids 1988;31:2491–503.
[7] Rashidi M, Hetstroni G, Banerjee S. Mechanisms of heat and mass transport at gas–liquid interfaces. Int J Heat Mass Transfer 1991;34:1799–805.
[8] Rashidi M. Burst-interface interactions in free surface turbulent flows. Phys Fluids 1997;9:3485–501.
[9] Volino RJ, Smith GB. Use of simultaneous IR temperature measurements and DPIV to investigate thermal plumes in a thick layer colled from above. Exp Fluids 1999;27:70–8.
[10] Komori S, Nagaosa R, Murakami Y, Chiba S, Ishii K, Kuwahara K. Direct numerical simulation of three-dimensional open-channel flow with zero-shear gas–liquid interface. Phys Fluids 1993;5:115–25.
[11] Pan Y, Banerjee S. A numerical study of free-surface turbulence in channel flow. Phys Fluids 1995;7:1649–64.
[12] Lombardi P, De Angelis V, Banerjee S. Direct numerical simulation of near-interface turbulence in coupled gas–liquid flow. Phys Fluids 1996;8:1643–65.
[13] Tsai W-T. A numerical study of the evolution and structure of a turbulent shear layer under a free surface. J Fluid Mech 1998;354:239–76.
[14] Nagaosa R. Direct numerical simulation of vortex structures and turbulent scalar transfer across a free surface in a fully developed turbulence. Phys Fluids 1999;11:1581–95.

[15] Handler RA, Saylor JR, Leighton RI, Rovelstad AL. Transport of a passive scalar at a shear-free boundary in fully developed turbulent open channel flow. Phys Fluids 1999;11:2607–25.
[16] Shen L, Triantafyllou GS, Yue DKP. Mixing of a passive scalar near a free surface. Phys Fluids 2001;13:913–26.
[17] Shen L, Zhang X, Yue DKP, Triantafyllou GS. The surface layer for free-surface turbulent flows. J Fluid Mech 1999;386:167–212.
[18] Germano M, Piomelli U, Moin P, Cabot W. A dynamic subgrid-scale eddy viscosity model. Phys Fluids 1991;3:1760–5.
[19] Smagorinsky J. General circulation experiments with the primitive equations. I. The basic experiment. Mon Wea Rev 1963;91:99–165.
[20] Wang W-P, Pletcher RH. On the large eddy simulation of a turbulent channel flow with significant heat transfer. Phys Fluids 1996;8:3354–66.
[21] Zang Y, Street RL, Koseff JR. A dynamic mixed subgrid-scale model and its application to turbulent recirculating flows. Phys Fluids 1993;5:3186–96.
[22] Calmet I, Magnaudet J. Large-eddy simulation of high-Schmidt number mass transfer in a turbulent channel flow. Phys Fluids 1997;9:438–55.
[23] Liu NY, Lu XY, Zhuang LX. A new dynamic subgrid-scale model for the large eddy simulation of stratified turbulent flows. Sci China A 2000;43:391–9.
[24] Zhong FQ, Liu NS, Lu XY, Zhuang LX. An improved dynamic subgrid-scale model for the large eddy simulation of stratified channel flow. Sci China A 2002;45:888–99.
[25] Dong YH, Lu XY, Zhuang LX. An investigation of Prandtl number effects on turbulent heat transfer in channel flows by large eddy simulation. Acta Mech 2002;159:39–51.
[26] Dong YH, Lu XY, Zhuang LX. Large eddy simulation of turbulent channel flow with mass transfer at high-Schmidt numbers. Int J Heat Mass Transfer 2003;46:1529–39.
[27] Salvetti MV, Zang Y, Street RL, Banerjee S. Large-eddy simulation of free-surface decaying turbulence with dynamic subgrid-scale models. Phys Fluids 1997;9:2405–19.
[28] Calmet I, Magnaudet J. Statistical structure of high-Reynolds-number turbulence close to the free surface of an open-channel flow. J Fluid Mech 2003;474:355–78.
[29] Kim J, Moin P. Application of fractional-step method to incompressible Navier–Stokes equations. J Comput Phys 1985;59:308–23.
[30] Verzicco R, Orlandi P. A finite-difference scheme for three-dimensional incompressible flows in cylindrical coordinates. J Comput Phys 1996;123:402–14.
[31] Verzicco R, Camussi R. Prandtl number effects in convective turbulence. J Fluid Mech 1999;383:55–73.
[32] Moin P, Kim J. Numerical investigation of turbulent channel flow. J Fluid Mech 1982;118:341–77.
[33] Na Y, Papavassiliou DV, Hanratty TJ. Use of direct numerical simulation to study the effect of Prandtl number on temperature fields. Int J Heat Fluid Flow 1999;20:187–95.
[34] Nagano Y, Shimada M. Development of a two-equation heat transfer model based on direct simulations of turbulent flows with different Prandtl numbers. Phys Fluids 1996;8:3379–402.
[35] Hsu CT, Lu XY, Kwan MK. LES and RANS studies of oscillating flows over a flat plate. ASCE J Engng Mech 2000;126:186–93.
[36] Wang L, Lu XY. An investigation of turbulent oscillatory heat transfer in channel flows by large eddy simulation. Int J Heat Mass Transfer 2004;47:2161–72.
[37] Dong YH, Lu XY. Large eddy simulation of a thermally stratified turbulent channel flow with temperature oscillation on the wall. Int J Heat Mass Transfer 2004;47:2109–22.
[38] Nagaosa R, Saito T. Turbulence structure and scalar transfer in stratified free-surface flows. AIChE J 1997;43:2393–404.
[39] Kader BA, Yaglom AM. Heat and mass transfer laws for fully turbulent wall flows. Int J Heat Mass Transfer 1972;15:2329–42.
[40] Kader BA. Temperature and concentration profiles in fully turbulent boundary layers. Int J Heat Mass Transfer 1981;24:1541–5.
[41] Kawamura H, Ohsaka K, Abe H, Yamamoto K. DNS of turbulent heat transfer in channel flow with low to medium-high Prandtl number fluid. Int J Heat Fluid Flow 1998;19:482–91.

[42] Kawamura H, Abe H, Matsuo Y. DNS of turbulent heat transfer in channel flow with respect to Reynolds and Prandtl number effects. Int J Heat Fluid Flow 1999;20:196–207.
[43] Shaw DA, Hanratty TJ. Turbulent mass transfer rates to a wall for large Schmidt number. AIChE J 1977;23:28–35.